18th International Conference on
TRANSPORT AND SEDIMENTATION OF SOLID PARTICLES
11-15 September 2017, Prague, Czech Republic
ISSN 0867-7964 ISBN 978-83-7717-269-8

FLOW VELOCITIES IN AN AXI-SYMMETRICAL ROTATING CUTTER SUCTION HEAD

B.J. Nieuwboer[1], G.H. Keetels, C. van Rhee

[1]PhD candidate, Faculty of Mechanical Engineering and Marine Technology, Delft University of Technology, Mekelweg 2, Delft, 2628 CD, E-mails: B.J.Nieuwboer@tudelft.nl, G.H.Keetels@tudelt.nl, C.vanRhee@tudelft.nl.

Although there have been many improvements in the design of cutter suction dredgers, a modern cutter still spills up to 40% of the cut rock in most unfavourable conditions. This spillage is the amount of rock that is cut loose by the cutter head, but is not sucked up by the dredge pump. This paper focusses on the flow phenomena of the water in the cutter. The flow partly causes this spillage. Previously, physical experiments have been performed to study the flow in a cutter head. In this paper the results of these measurements are used for the validation of an unsteady flow model. The cutter is modelled using Computational Fluid Dynamics with the OpenFOAM software. The modelled fluid velocities are averaged over one revolution and are compared with the time averaged velocities from experiments. This shows good agreement for different rotational speeds of the cutter head.

KEY WORDS: Cutter Suction Dredger, Numerical Modelling, Spillage, OpenFOAM

1. INTRODUCTION

A cutter suction dredger dredges sand, clay and rock. The cutter suction dredger uses a rotating cutter head (Figure 1a) for cutting the soil and transporting using the dredge pump to the vessel. Figure 1b shows a schematic of a cutter suction dredger. The dredging vessel rotates around the spud pole by pulling itself with anchor lines on each side of the vessel (not shown in the figure). The cutter head, shown in grey, cuts the soil. The dredge head creates a breach in the soil and sucks up the soil that is cut loose. When the dredger has swung to its extreme position, the vessel moves forward by pushing the anchor pole backward. Then the vessel swings to the other side until it has swung to its extreme position again. This process is repeated.

A dredger wants to remove all the soil, which is cut loose by the dredge head. However, up to 40% is not sucked up to the vessel when cutting rock. This spillage can be separated into two parts. The first part are the pieces of rock which are cut, but never enter the cutter head. These pieces are pushed away, due to the cutting process and therefore do not enter

the cutter head. The second type of spillage are the pieces of rock which do enter the cutter, but are thrown out of the cutter due gravity, centrifugal forces and outward fluid flow.

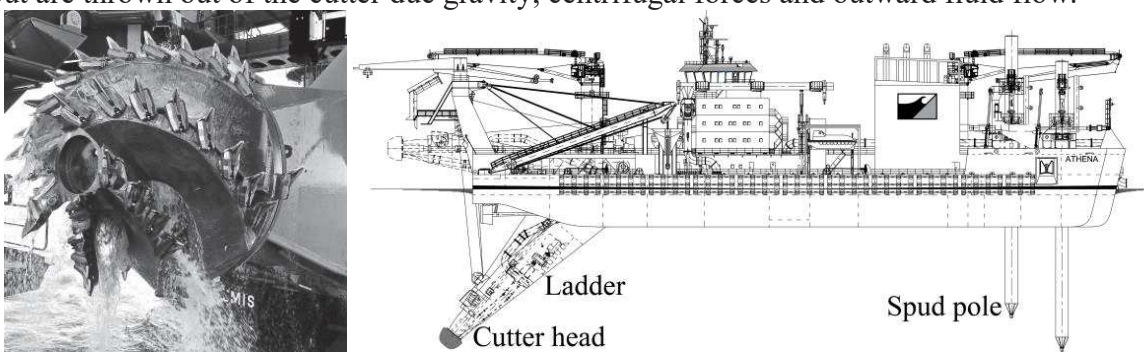

a) b)

Fig. 1 A cutter head used for dredging rock (a). A schematic drawing of a cutter suction dredger, called Athena owned by van Oord (b)

This paper considers the fluid flow in the cutter, which is partly responsible for the spillage. In the future this flow model will be used for the modelling of the spillage of the cutter. The fluid flow is studies using a numerical model of a simplified axi-symmetrical cutter. The results of this model are compared with previously performed experiments.

2. PREVIOUS STUDIES

Dekker (2003) performed velocity measurements in a cutter with back plate and suction mouth and compared the velocities with a potential flow solver. He considered steady state conditions only. However, it can be anticipated, that transient effects are important. Due to their curved shape, the rotating blade blades scoop up the particles and transport them to the suction mouth. The pieces of rock also do not get inside the cutter at a constant rate in time. The blades scoop up the pieces. This creates a periodicity in the input of rock to the cutter. This shows the need for an unsteady modelling approach.

Also, the transient flow phenomena are important. When the suction mouth is not placed axi-symmetrical, the moving blades past the suction flow, induce a secondary flow. The passing of the blades also induce some velocity oscillations in the rest of the domain. For these four reasons this study towards the fluid flow uses an unsteady approach.

3. EXPERIMENTAL SET-UP

Before the study of Dekker (2003), the same author measured the flow velocities inside a cutter without a back plate (Figure 2a). In this schematic 1:4 model cutter the velocities were measured at 5 locations. These locations are shown together with the results in figure 3 and 4. The set-up is axi-symmetrical. Therefore one only needs to measure at a single azimuthal coordinate for determining the flow phenomena.

The flow inside a cutter head can be characterized by a dimensionless inverse flow number ($\theta^{-1} = \omega R^3/Q$). This is the ratio between the rotational velocity of the cutter head (ωR) and the suction discharge (Q). This flow number originates from the dimensional

analysis of centrifugal pumps. Steinbusch (1999) was the first to use this for rotating cutter heads. During operational conditions, the inverse flow number has typical values between 1.6 and 3.7.

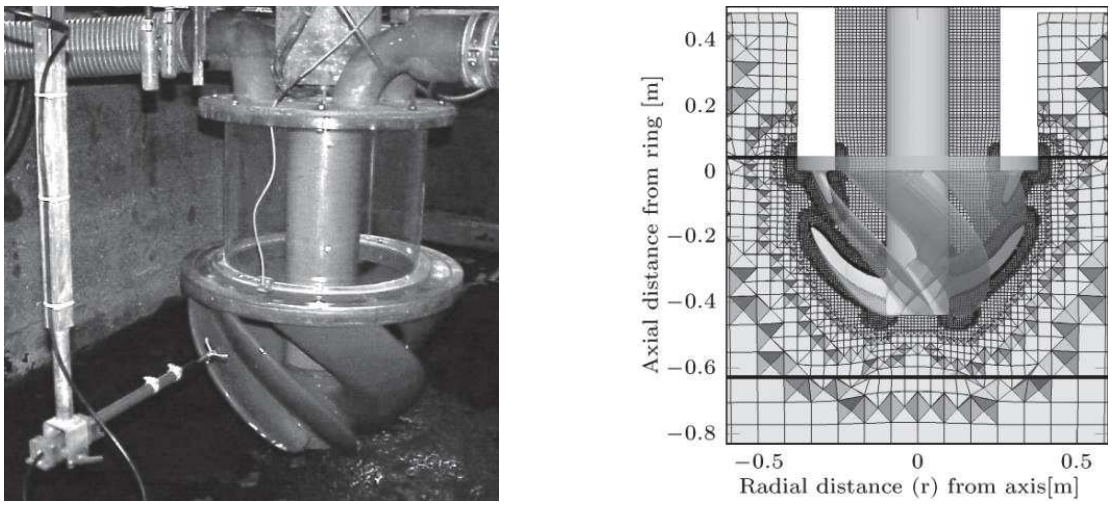

a) b)

Fig. 2 The experimental setup (a) and numerical mesh (b)

The main author of Dekker (2003) measured the velocities in the axi-symmetric model cutter using an Acoustic Doppler Velocimeter (ADV). This ADV has a sampling frequency of 25 Hz and measured the 3 velocity components in 3 directions. Figure 2a shows the ADV in the left downward corner.

The velocity data, obtained from using the ADV, includes some spikes in the signal. Goring and Nikora (2002) described an algorithm to determine whether these spikes are likely due to errors in the measuring technique. When the acceleration of the fluid is higher than the gravitational acceleration or when the strength of the acoustic signal is too low, the data is discarded.

4. UNSTEADY CFD MODEL

The end goal of the numerical model is to predict the spillage of rock pieces. For this purpose the velocities inside the cutter need to be computed. The flow is mainly driven by pressure of the suction and the displacement of water by the blades.

The pieces of rock are relatively large, which means that the smallest velocity fluctuations won't have an influence. This, together with the pressure as driving force, justifies the use of the Unsteady Reynolds Averaged Navier Stokes equations for solving the flow inside the cutter. In these equations the turbulent fluctuations are modelled in a time averaged way. This means velocities on the larger time scales are solved and the small time scales are modelled using a turbulence model. In this case the flow velocities due to the passing of the blades are still solved.

The Unsteady Reynolds Averaged Navier Stokes equations are solved using a Finite Volume method. This discretisation method is widely used for complex geometries and rotating machinery. To solve the fluid flow, the authors use the open source package,

OpenFOAM 1606+ (www.openfoam.com). In this modelling environment the methods for solving the Raynolds Averaged Navier-Stokes equations are already implemented.

The rotating motion of the blades is solved using a sliding mesh method. This method is available in all the modern OpenFOAM versions. One mesh fits arounds the blades and rotates together with them. The rest of the geometry and mesh are standing still. The mesh needs to slide over an interface. The values on this interface are interpolated from the non-rotational to the rotational domain in a mass and momentum conservative way, Farrell (2011). The thick black line in Figure 2b shows part of this interface.

The pressure and velocities are solved using the PISO algorithm. (Weller 2005). The turbulence of the fluid is modelled with an unsteady k-omega SST model.

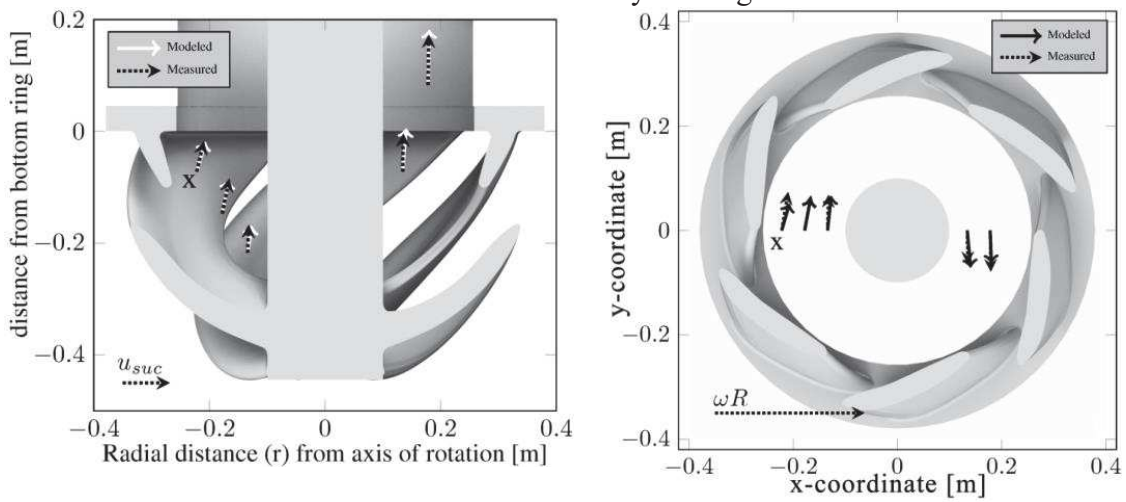

Fig 3. Front and bottom view view of the measured and modelled time averaged velocities in the cutter

The numerical domain is a cylinder with a diameter of 5 meter and a height of 1.31 meter, which consists out of 8.87 cells. In both the experiments and simulation the cutter was positioned 0.39 meter above the bottom. The height of the domain matches the approximate height of the water level in the experiments. The water in the simulation has a density of 1000 kg/m^2 and a kinematic viscosity of $1.0 \cdot 10^{-6}$ m^2/s.

The top and bottom of the cylindrical domain have a no slip boundary. The inlet is located at the circumference of the cylinder and has a Dirichlet boundary. The boundary at outflow at the top of the suction pipe is a Neumann boundary. The turbulent quantities at the inlet are computed on forehand using a steady simulation of the cutter. Turbulent kinetic energy $k = 1.1 \cdot 10^{-6}$ m^2/s^2, specific dissipation $\omega = 4.1 \cdot 10^{-2}$ s^{-1} and turbulent viscosity $\upsilon_t = 2.6 \cdot 10^{-5}$m^2/s.

The mesh size inside the cutter is 1 cm^3 and at the blades the mesh is 4 mm3. The advection term is discretized using a 70% central interpolation scheme and 30% upwind. The upwind interpolation causes some numerical diffusion. However, this is needed to keep the solution stable.

All the models use a maximum courant number of 1. The time step is limited by this courant number. In the simulations described in the next sections, the time steps differs between $2.5 \cdot 10^{-4}$ and $7.5 \cdot 10^{-4}$ seconds.

The authors simulated some cases with different numerical settings to see the influence of these. The time step was lowered with a factor 3.3, the mesh was refined so each cell length was 25% smaller. This increased the mesh to 1.8 million cells

Also the convergence criteria of the matrix solution were lowered. These cases gave a similar results for the developed flow. For each velocity component the 5 described points the maximum difference with the base mesh was taken. When the time step is lowered the average difference to the base mesh is $9.6 \cdot 10^{-3}$ m/s. Refining the mesh gives a bit larger difference from the base case: $2.9 \cdot 10^{-2}$ m/s.

5. RESULTS

This section shows the results for 6 different rotating velocities with a fixed suction discharge. Every model is first initialized using a steady simulation. Afterwards, the cutter is rotated 6 revolutions. The average velocities presented are based upon the last revolution. The inverse flow numbers of these simulations extent from 0 to 3.5.

5.1 TIME AVERAGED RESULTS

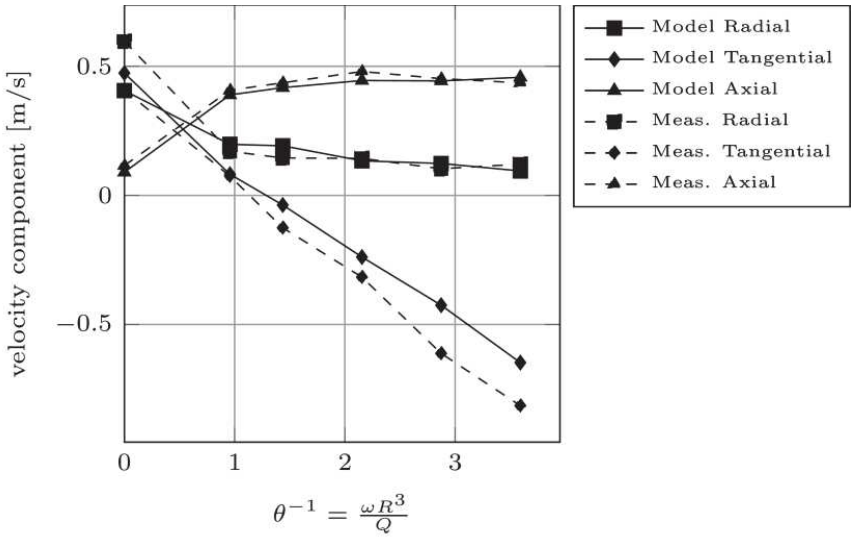

Fig 5. Modelled and measured velocities components versus inverse flow number at point x

Figure 3 and 4 show the modelled and measured time averaged velocities in the cutter for an inverse flow number $\theta^{-1} = 2.9$. In both figures the cutter head has been cut to visualise the geometry in relation to the velocities. The measured velocities are shown in dotted arrows, the modelled velocities as an unbroken line.

Figure 3 shows the cut of the r-z plane with the velocities. The modelled and measured velocities line up well. One can see that the velocities at the locations near the blade get pushed inward a bit. This is due to the shape of the blade. The magnitude of the velocities has the same order of magnitude as the average suction velocity depicted by the arrow in the left downward corner.

Figure 4 shows an azimuthal plane with the velocities, viewed from the tip of the axis. The modelled velocities at the left side show a bit more shear than the measured velocities.

At these points the magnitude of the velocities are around a third of the velocity at the outside of the ring (depicted by the arrow labelled ωR)

For the measurement location 'x' in Figure 3 and 4, the measured velocity is plotted against the inverse flow number (Figure 5). When the cutter is not rotating, the inverse flow number is zero. In this situation the flow in the cutter is reversed from the flow forced by the rotating blades. This corresponds with a counter clockwise flow in figure 4 and a positive tangential velocity in Figure 5. The flow reversal is caused by angle between the blades and the tangent of the rotating motion of the cutter. With a higher rotation the tangential velocity starts rotating clockwise. Figure 5 shows a linear relationship between the inverse flow number and the tangential velocity.

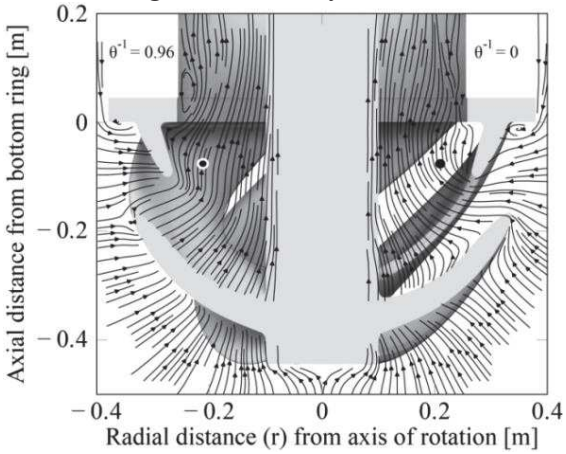

Fig 6. Modelled instantaneous streamlines of the velocity for $\theta^{-1} = 0$ (right side) and $\theta^{-1} = 0.96$ (left side)

The radial and axial velocities change much less with increasing rotation than the tangential velocities. The positive radial velocity is defined towards the cutter axis and the positive axial flow towards the suction mouth. Figure 5 shows that the radial component decreases with increasing rotation. This is likely caused due to the outward pointing centrifugal forcing on the flow. A second contribution is the increasing axial velocity at the tip of the axis with increasing angular velocity. Due to the shape of the blades at this location the water is pushed upward. Since the suction discharge is kept constant, this water should leave the cutter again. This could also explains the slightly increasing axial velocities with higher angular velocity.

When the cutter does not rotate, the radial velocity is much higher and the axial velocity is much lower. Figure 6 shows the instantaneous modelled streamlines of the flow for $\theta^{-1} = 0$ (right halve of the figure 6) and θ^{-1} =0.96 (left side of the picture). The two black dots represent the measuring location of the data from figure 5. In the case with no rotation. The fluid has to move around the blades leading to a higher radial flow. Because the flow has a more inward direction the axial velocity is relatively low.

5.2 MODEL PERFORMANCE

In Figure 7 the velocities components from all 6 operational conditions are compared with the experiments. Nearly all points are within an error band of 25%. In table 1 the

model performance is computed using the Mean Absolute Error and the Mean Absolute Percentage Error (using equation 2). The tangential and axial velocity components are computed well. The radial component is harder to predict.

$$\text{MAE} = \frac{1}{n}\sum_{i=1}^{n}|d_i - m_i| \qquad \text{MAPE} = \frac{1}{n}\sum_{i=1}^{n}\frac{|d_i - m_i|}{d_i} \qquad (1,2)$$

Where n is the number of data samples, d_i is the data value (measured) and m_i is the modelled value.

Table 1

Model performance based upon the MAE and MAPE for all 6 operational conditions

	Radial	Tangential	Axial
MAE	0.049 m/s	0.11 m/s	0.046 m/s
MAPE	46.2%	17.1%	8.7%

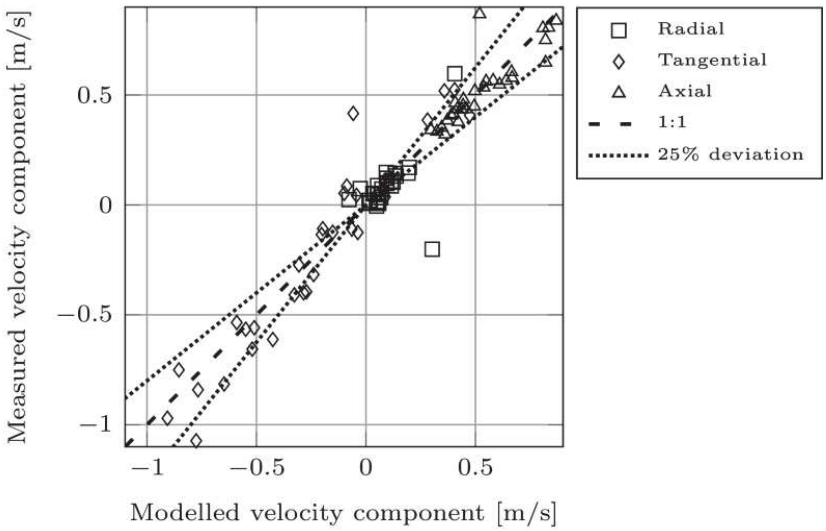

Fig 7. Measured versus modelled velocities per velocity component

5.3 UNSTEADY FLOW NEAR THE RING

Burger (2003) describes that one of spillage mechanisms are the particles that leave the cutter near the ring. The question is whether the unsteady local fluid velocities contribute to this spillage. At 5 cm under the ring and near the blades, the radial velocity oscillates with an amplitude of 0.3 to 0.4 m/s around a zero velocity. This means that water flows also out of the cutter at this location. By determining the response factor of the particles on this fluid fluctuation, it can be shown that this oscillation has a significant effect on the particles. Keetels (2017) rewrote the formulation (Equation 3) for the response factor (C_t) for a particles in an oscillating fluid by Hill (1998) and others. He came up with an expression based on the response times of the fluid eddy and particles (τ_f, τ_p), the densities of the fluid and the particles (ρ_f, ρ_s) and the added mass coeficint (C_A), which is typically 0.5. It is assumed that the response is driven by inertia, drag, added mass and a pressure gradient. For a response factor of 1 the particle would be accelerated as much as the surrounding water. For a very dilute concentration this expression is:

$$C_t = \frac{\frac{\rho_f}{\rho_s} + (1 + C_A) + \frac{\tau_f}{\tau_p}}{\left(1 + C_A \frac{\rho_f}{\rho_s}\right) + \frac{\tau_f}{\tau_p}} \quad (3)$$

The density of water and the sediment are taken respectively 1000 k/m^3 and 2500 k/m^3. The fluid time scale is related to the blade passing frequency. This would be typically 0.13 s on model scale. For this model cutter, the scaled median particle size is around 2 cm. The particle response time based on the fall velocity is 0.098 s. This is computed using a terminal fall velocity of 0.96 m/s. With these data a response factor of 0.79 can be computed. This means that the water movement caused by the passing of the blades does accelerate the particles outward. And thus has an influence on the spillage.

6. CONCLUSION

The proposed model to simulate the flow velocities in a rotating cutter head performs well. It can compute the velocities within an error margin of around 25%. This gives the confidence that this flow model can serve as a basis for computing the spillage in a cutter. The velocity oscillations by the blades passing have an influence on the particles in the cutter near the ring.

ACKNOWLEDGEMENTS

The authors would like to thank Royal Boskalis Westminster and Van Oord Dredging and Marine Contractors for their financial support.

REFERENCES

1. Burger, M. D. (2003). Mixture forming processes in dredge cutterheads (Doctoral dissertation, Ph. D. dissertation, Delft Univ. of Technology, Delft, Netherlands).
2. Dekker, M. A., Kruyt, N. P., Den Burger, M., & Vlasblom, W. J. (2003). Experimental and numerical investigation of cutter head dredging flows. Journal of waterway, port, coastal, and ocean engineering, 129(5), 203-209.
3. Farrell, P. E., & Maddison, J. R. (2011). Conservative interpolation between volume meshes by local Galerkin projection. Computer Methods in Applied Mechanics and Engineering, 2001, 89-100.
4. Goring, D. G., & Nikora, V. I. (2002). Despiking acoustic Doppler velocimeter data. Journal of Hydraulic Engineering, 128(1), 117-126.
5. Hill, D. P. (1998). The computer simulation of dispersed two-phase flow (Doctoral dissertation, University of London).
6. Keetels, G. H., Goeree, J. C., & van Rhee, C. (2017). Advection-diffusion sediment models in a two-phase flow perspective. Journal of Hydraulic Research, 1-5.
7. Steinbusch, P. J., Vlasblom, W. J., den Burger, M., & Kruyt, N. P. (1999). Numerical simulation of the flow generated by cutter heads. In BHR GROUP CONFERENCE SERIES PUBLICATION (Vol. 36, pp. 435-444). Bury St. Edmunds; Professional Engineering Publishing; 1998.
8. Weller, H. (2005). Pressure-velocity solution algorithms for transient flows. Technical Report TR/HGW/05, OpenCFD Ltd.